



1 **Winter brown carbon over six China's megacities: Light**
2 **absorption, molecular characterization, and improved**
3 **source apportionment revealed by multilayer perceptron**
4 **neural network**

5 Diwei Wang¹, Zhenxing Shen^{1*}, Qian Zhang², Yali Lei³, Tian Zhang¹, Shasha Huang¹,
6 Jian Sun¹, Hongmei Xu¹, Junji Cao⁴

7 ¹Department of Environmental Science and Engineering, Xi'an Jiaotong University, Xi'an 710049,
8 China

9 ²Key Laboratory of Northwest Resource, Environment and Ecology, MOE, Xi'an University of
10 Architecture and Technology, Xi'an 710055, China

11 ³Key Lab of Geographic Information Science of the Ministry of Education, School of Geographic
12 Sciences, East China Normal University, Shanghai 200241, China

13 ⁴Key Lab of Aerosol Chemistry & Physics, SKLLQG, Institute of Earth Environment, Chinese Academy
14 of Sciences, Xi'an, China

15 *Correspondence to:* Zhenxing Shen (zxshen@mail.xjtu.edu.cn)

16 **Abstract.** Brown carbon (BrC) constitutes a large fraction of organic carbon and exhibits strong light
17 absorption properties, thus affecting the global radiation budget. In this study, we investigated the light
18 absorption properties, chemical functional bonds, and sources of BrC in six megacities in China, namely
19 Beijing, Harbin, Xi'an, Chengdu, Guangzhou, and Wuhan. The average values of the BrC light
20 absorption coefficient and the mass absorption efficiency at 365 nm in northern cities were higher than
21 those in southern cities by 2.5 and 1.8 times, respectively, demonstrating the occurrence of abundance of
22 BrC in northern China's megacities. Fourier transform-infrared (FT-IR) spectra revealed sharp and
23 intense peaks at 1640, 1458–1385, and 1090–1030 cm⁻¹, which were ascribed to aromatic phenols,
24 confirming the contribution of primary emission sources (e.g., biomass burning and coal combustion) to
25 BrC. In addition, we noted peaks at 860, 1280–1260, and 1640 cm⁻¹, which were attributed to
26 organonitrate and oxygenated phenolic groups, indicating that secondary BrC also existed in six
27 megacities. Positive matrix factorization (PMF) coupled with multilayer perceptron (MLP) neural
28 network analysis were used to apportion the sources of BrC light absorption. The results showed that
29 primary emissions (e.g., biomass burning, tailpipe emissions, and coal combustion) made a major
30 contribution to BrC in six megacities. However, secondary formation processes made a greater



31 contribution to light absorption in the southern cities (17.9%–21.2%) than in the northern cities (2.1%–
32 10.2%). These results can provide a basis for the more effective control of BrC to reduce its impacts on
33 regional climates and human health.

34 **1 Introduction**

35 Brown carbon (BrC) constitutes a vital fraction of carbonaceous aerosols and exhibits strong light
36 absorption properties in near-ultraviolet (UV) and visible wavelength regions (Laskin et al., 2015; Wu et
37 al., 2021; Zhang et al., 2022). Therefore, it has received extensive attention in recent years (Laskin et al.,
38 2015; Yan et al., 2018; Yuan et al., 2020). BrC has substantial effects on radiative forcing, cloud
39 condensation, ice cores, and climate (Ma et al., 2020; Sreekanth et al., 2007). On the basis of remote
40 sensing observations and chemical transport model results, studies have detected a BrC-induced
41 nonnegligible positive radiative forcing ranging from 0.1 to 0.6 W m⁻² on a global scale (Jo et al., 2016;
42 Wu et al., 2020).

43 BrC in urban atmospheres can originate from numerous sources, including incomplete combustion of
44 fossil fuels, biomass burning, forest fires, and residential coal combustion (Kirchstetter et al., 2004; Shen
45 et al., 2017; Soleimanian et al., 2020). In addition, both primary BrC and gaseous pollutants emitted from
46 anthropogenic and biological activities can be converted into secondary BrC through a series of
47 atmospheric chemical reactions (Kumar et al., 2018; Laskin et al., 2015). Studies have determined that
48 the absorption properties of BrC exhibited distinct temporal and spatial variations in different regions
49 and cities, and these properties were closely related to diverse emissions sources and complex
50 atmospheric aging processes (Chung et al., 2012; Wu et al., 2021). For example, Devi et al (2016)
51 observed that BrC contributed differently to light absorption in the rural and urban southeast United
52 States. Furthermore, a stronger light absorption ability in cold seasons (fall and winter) in Beijing, Xi'an,
53 Taiyuan, Seoul, and other cities has been found to be strongly associated with increased biomass burning
54 emissions (Cheng et al., 2016; Kim et al., 2016; Mo et al., 2021; Shen et al., 2017). Another study noted
55 that secondary organic aerosol (SOA) formation processes constituted a major source of BrC in Atlanta
56 and Los Angeles; moreover, the optical properties of BrC differed considerably between the two cities
57 due to differences in secondary BrC precursors (Zhang et al., 2011).

58 China has a high concentration of atmospheric water-soluble organic carbon, which has a major impact

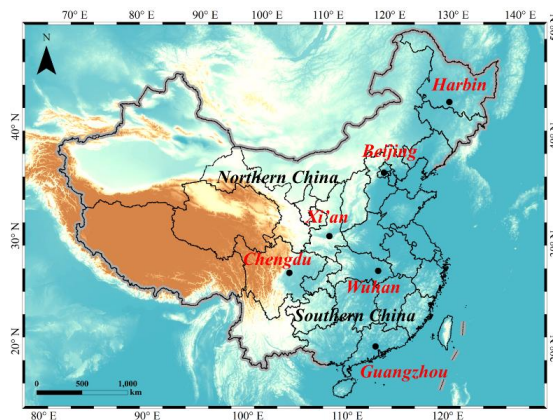


59 on regional air quality, visibility, and the climate (Mo et al., 2021). However, to our knowledge, limited
60 study was conducted to insight to the optical profiles, molecular composition, and sources apportionment
61 of BrC in a large scale in China. Accurately understanding the spatial variations of the sources and light
62 absorption properties of BrC in China is essential for reducing uncertainty about the effects of BrC on
63 the climate. Many studies have used receptor modelling techniques such as positive matrix factorization
64 (PMF) coupled with multiple linear regression analysis to assign the sources of BrC (Bao et al., 2022;
65 Lei et al., 2019; Soleimani et al., 2020). However, atmospheric processes are generally non-linear in
66 nature, thus traditional deterministic models could be limited. The artificial neural network (ANN) based
67 models, such as multilayer perceptron (MLP), have been shown to provide meaningful results closer to
68 realistic estimates than most linear models (Borlaza et al., 2021; Elangasinghe et al., 2014). Therefore,
69 in this study, a winter campaign for PM_{2.5} sampling was conducted over six China's megacities. The
70 purposes of this study were to 1) investigate the spatial variations of the carbonaceous matter
71 concentrations and optical properties of BrC across six representative urban areas in China, 2) determine
72 the molecular composition of BrC, and 3) insight the relationship between light absorption and BrC
73 sources by using PMF coupled with ANN-MLP.

74 **2 Methods**

75 **2.1 Samples collection**

76 PM_{2.5} samples were collected in six cities in China (Figure 1): three cities in northern China (Beijing
77 [BJ], Harbin [HrB], and Xi'an [XA]) and three cities in southern China (Chengdu [CD], Guangzhou
78 [GZ], and Wuhan [WH]). We classified the cities as being in northern or southern cities according to their
79 geographic location, such as "north or south of the Huaihe River". Owing to geographical factors, these
80 cities exhibit considerable differences in terms of energy structure and climate. The average annual
81 temperature in northern cities is generally below 15°C, while in southern cities it is usually above 15°C
82 (Mo et al., 2021). Information about the six cities and the sampling sites is summarized in Table S1
83 (Supporting Information).



84

85 **Figure 1. PM_{2.5} samples were taken in six Chinese cities.**

86

87 For sample collection, filter samplers were mounted on rooftops between 8 and 30 m above the ground,
88 and samples were collected from November 20 to December 22, 2019. In BJ, HrB, and GZ, a mini-
89 volume sampler operating at 5 L min⁻¹ (Airmetrics, Springfield, OR, USA) was used to collect PM_{2.5}
90 samples on 47-mm quartz-fiber filters (Whatman, Maidstone, UK) for 24 h. In CD, a medium-volume
91 PM_{2.5} sampler operating at 100 L min⁻¹ (HY-100SFB, Hengyuan, Qingdao, China) was used to collect
92 PM_{2.5} samples on 90-mm quartz-fiber filters (Whatman). Moreover, in XA and WH, a high-volume
93 sampler (HVS-PM_{2.5}, Thermo-Anderson Inc. Cleves, OH, USA) with a flow rate of 1.13 m³ min⁻¹ was
94 used to collect PM_{2.5} samples on quartz-fiber filters (203 mm × 254 mm, Whatman, QMA). Before
95 sample collection, all quartz filters were prebaked at 780 °C for 7 h to eliminate any residual carbon. A
96 detailed description of the quality control procedures for the filters before and after the sampling
97 processes can be found in the article by Shen et al (2017). After the sampling processes, the samples were
98 sealed and stored below 0 °C to avoid evaporative losses before analysis.

98

2.2 Chemical analysis

99

100 The organic carbon (OC) and elemental carbon (EC) of the PM_{2.5} samples were analyzed using a
101 Thermal and Optical Carbon Analyzer (DRI Model 2001A, Atmoslytic, Inc., USA) in accordance with
102 the improved Interagency Monitoring of Protected Visual Environment (IMPROVE) thermal/optical
103 reflectance protocol. Detailed descriptions of the OC and EC measurement methods can be found in the
104 article by Cao et al (2004). A portion of each filter (about 2.84 cm²) was extracted using 10 mL of
ultrapure water to analyze water-soluble inorganic ions (Na⁺, NH₄⁺, K⁺, Mg²⁺, Ca²⁺, Cl⁻, NO₃⁻, and SO₄²⁻)



105 through ion chromatography (Dionex 500, Dionex Corp, USA). A detailed description of the ion analysis
106 method used in this study can be found in the article by Shen et al (2008).

107 **2.3 Optical properties of methanol extracts**

108 A 0.526-cm² punch was ultrasonically extracted from each filter sample by using 5 mL of methanol
109 (HPLC Grade, Fisher Scientific, NH, USA) for 30 min. Subsequently, all extracts were filtered through
110 a microporous membrane with a diameter of 25 mm and pore size of 0.22 μm (Puradisc 25 TF, PTFE
111 membrane) to remove insoluble components. The UV–visible absorption spectra of the BrC samples
112 were determined using a liquid waveguide capillary cell–total OC spectrophotometer (LWCC-2100,
113 World Precision, Sarasota, FL, USA) between the wavelengths of 200 and 700 nm. The BrC optical
114 properties such as $b_{abs365, methanol}$ (The absorption coefficient for methanol extracts at 365 nm) and $MAE_{365, methanol}$
115 (normalized by $b_{abs365, methanol}$ to organic carbon, OC) were calculated as showed in previous study
116 (Lei et al., 2019) and details was listed in Text S1.

117 **2.4 Fourier transform infrared spectroscopy spectra**

118 Functional groups in the samples collected in six megacities were characterized using a Fourier
119 transform infrared (FT-IR) spectrometer (Bruker Optics, Billerica, MA, USA). The method described in
120 section 2.3 was used to extract the BrC filtrates, then the BrC extracts were concentrated to 0.5 mL under
121 a gentle nitrogen flow, after which they were mixed with 0.2 g of KBr (FT-IR grade, Sigma-Aldrich) and
122 then blown with nitrogen to complete dryness. The resulting extract–potassium bromide mixture was
123 ground in an agate mortar and examined through FT-IR spectroscopy. The FT-IR spectrum of each sample
124 was recorded in transmission mode by averaging 64 scans using a standard optical system with KBr
125 windows. The spectra were recorded in the wavelength range of 4000–400 cm⁻¹ at a resolution of 4 cm⁻¹.
126 Before analyzing the aerosol extract samples, we obtained the baseline spectrum by analyzing pure KBr.

127 **2.5 Source apportionment of BrC light absorption coefficient at 365 nm**

128 In this study, the source apportionment of BrC was conducted using the PMF coupled with ANN-MLP
129 methods by following the steps: 1) identification and quantification of the major sources of PM_{2.5} for the
130 six cities using PMF (The United States Environmental Protection Agency, PMF 5.0); 2) produces a
131 predictive model by ANN-MLP for one variable (BrC b_{abs365}) based on the values of the input variables



132 (PM_{2.5} sources daily contributions). PMF is a bilinear factor model that has been widely used in source
133 apportionment studies (Shen et al., 2010; Cao et al., 2012; Lei et al., 2018; Li et al., 2021; Tao et al.,
134 2017). In the present study, water-soluble inorganic ions (Na⁺, NH₄⁺, K⁺, Mg²⁺, Ca²⁺, NO₃⁻, SO₄²⁻ and
135 Cl⁻) and carbon fractions (OC1, OC2, OC3, OC4, EC1, and EC2) were used as data inputs for PMF. The
136 PMF model was run multiple times, extracting four to six factors. A more detailed description of these
137 items can be found in the article by Lei et al (2019). Subsequently, an MLP model was constructed. The
138 model was developed using IBM SPSS Statistics for Windows, version 23 (IBM Corp., Armonk, NY,
139 USA). The detail information of the ANN-MLP model construction and training was described in Text
140 S2. After ANN-MLP model training, the obtained MLP model was applied to a set of virtual datasets.
141 Each virtual dataset consists of each source with the same mass contribution (from PMF analysis) as the
142 original dataset, but with one source set to zero. The $b_{\text{abs}365}$ contribution for a specific source was obtained
143 by subtracting the $b_{\text{abs}365}$ simulation value obtained using the virtual dataset from the $b_{\text{abs}365}$ simulation
144 value obtained using the original MLP model, which contains all the source contributions (Borlaza et al.,
145 2021).

146 **3 Results and discussion**

147 **3.1 General description of PM_{2.5} and its chemical species in six megacities**

148 As presented in Table S2, the PM_{2.5} concentrations in six cities ranged from 9.9 to 241.9 µg/m³ and
149 exhibited a significant spatial variation ($p < 0.01$), indicating the complexity of air pollution and spatial
150 differences in air pollution levels in China. HrB had the highest average PM_{2.5} concentration (85.5 ± 43.9
151 µg/m³), which exceeded National Air Quality Standard grade-II (24-h average: 75 µg/m³) and was 1.5,
152 1.1, 1.2, 2.0 and 1.3 times higher than those recorded in BJ, XA, CD, GZ, and WH, respectively. This
153 phenomenon indicates that PM_{2.5} pollution is still a major challenge in China, particularly in northern
154 China.

155 The average concentration of OC, a major chemical component of PM_{2.5}, ranged from 5.6 to 19.4
156 µg/m³ in six megacities; these cities can be arranged (in descending order) as follows in terms of the
157 average OC concentration: HrB > XA > BJ > WH > GZ > CD (Table S2). Similar to the trend observed
158 for PM_{2.5}, the average OC concentration in the northern cities (15.5 ± 7.9 µg/m³) was higher than that in
159 the southern cities (9.2 ± 4.6 µg/m³); this can primarily be attributed to substantial emissions from



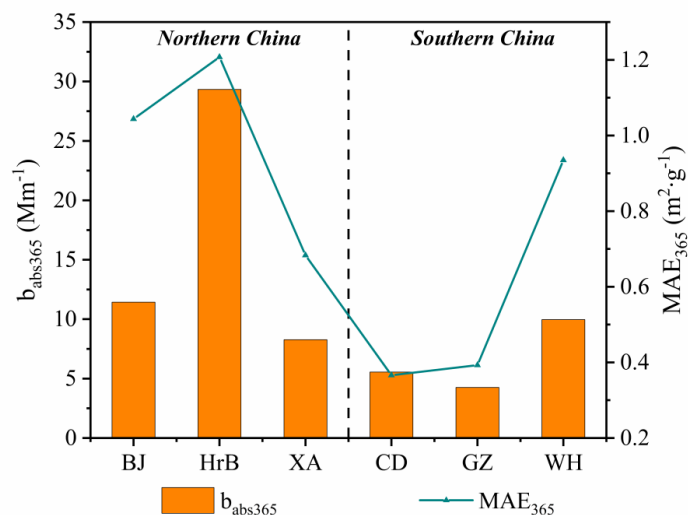
160 residential heating in winter in northern China (Lei et al., 2018; Sun et al., 2017; Zhang et al., 2021). To
161 assess the sources of atmospheric BrC, we estimated the concentrations of primary OC (POC) and
162 secondary OC (SOC) by using the EC tracer method (Ram and Sarin, 2011). As presented in Table S2,
163 the average SOC concentrations throughout the measurement period ranged from 1.0 (CD) to 9.2 $\mu\text{g}/\text{m}^3$
164 (HrB), and the fractional contributions of SOC to OC varied from 22.6% to 66.6%. The average POC
165 concentrations ranged from 4.0 (GZ) to 10.2 $\mu\text{g}/\text{m}^3$ (HrB), and POC constituted 34.4%–77.4% of the
166 total OC mass in the six cities. Accordingly, the SOC and POC concentrations exhibited typical spatial
167 fluctuations, which were consistent with the fluctuations of the $\text{PM}_{2.5}$ and total OC concentrations. These
168 results reveal that primary emissions usually dominated secondary formation processes, especially in the
169 northern cities.

170 3.2 Light absorption properties of BrC

171 As plotted in Figure 2, the light absorption coefficient (b_{abs} , Mm^{-1}) values for BrC exhibited significant
172 spatial variations across the six cities (1.7–64.1 Mm^{-1} ; $p < 0.01$). We executed Student t test at the 95%
173 confidence level and observed that HrB had the highest average $b_{\text{abs}365}$ value ($29.3 \pm 14.2 \text{ Mm}^{-1}$),
174 followed by BJ ($11.4 \pm 3.9 \text{ Mm}^{-1}$), WH ($10.0 \pm 3.2 \text{ Mm}^{-1}$), XA ($8.3 \pm 2.4 \text{ Mm}^{-1}$), CD ($5.6 \pm 2.7 \text{ Mm}^{-1}$),
175 and GZ ($4.3 \pm 1.4 \text{ Mm}^{-1}$). The average $b_{\text{abs}365}$ value in the northern cities was $15.7 \pm 12.3 \text{ Mm}^{-1}$, which
176 was 2.5 times higher than that in the southern cities ($p < 0.01$). The large variation in the measured $b_{\text{abs}365}$
177 values in these megacities was observed, which reflected that the light absorption of BrC was heavily
178 affected by chromophore sources (Huang et al., 2018; Soleimanian et al., 2020), aging during
179 atmospheric transportation (Lambe et al., 2013), and meteorological conditions (Li et al., 2021). Light-
180 absorbing carbonaceous aerosols were believed to be responsible for the considerable absorption of light
181 in the atmosphere (Xie et al., 2020). As presented in Figure S2, we observed positive correlations between
182 $b_{\text{abs}365}$ and POC in the six cities (r range: 0.61–0.92). Similar correlations were observed between $b_{\text{abs}365}$
183 and SOC (r range: 0.51–0.80), indicating that the sources of atmospheric BrC in the six cities were quite
184 complex. Apart from primary emissions, secondary formation processes also seemed to have a
185 considerable contribution to BrC in these cities. The $b_{\text{abs}365}$ values in HrB, BJ, XA, and WH are within
186 the range of values observed previously in Beijing (4–75 Mm^{-1} ; Cheng et al., 2016) and the Indo-
187 Gangetic Plain (3–457 Mm^{-1} ; Satish et al., 2020). Biomass burning was revealed to be the dominant
188 source of BrC in these cities during winter (Elser et al., 2016; Shen et al., 2009; Sun et al., 2017).



189 Furthermore, we observed high correlations (r range: 0.69–0.92) between $b_{\text{abs}365}$ and K^+ , which is
190 commonly regarded as a tracer of biomass burning (Shen et al., 2010), in HrB, BJ, XA, and WH (Figure
191 S3). This evidence supports the aforementioned findings that emissions from biomass burning might be
192 the major BrC source in winter in these cities. For the southern cities CD and GZ, the low $b_{\text{abs}365}$ values
193 ($1.7\text{--}11.5 \text{ Mm}^{-1}$) are of the same order of magnitude as those reported previously in Nanjing ($3.3\text{--}13$
194 Mm^{-1} ; Chen et al., 2019; Chen et al., 2018), Seoul ($0.9\text{--}7.3 \text{ Mm}^{-1}$; Kim et al., 2016), and Hong Kong
195 ($4.8\text{--}10.6 \text{ Mm}^{-1}$; Zhang et al., 2020). The aging or oxidation of aerosols was confirmed to be the major
196 source of BrC in these regions, indicating that secondary aerosols are likely a major source of winter BrC
197 in CD and GZ.



198

199 **Figure 2. Spatial variations of BrC light absorption properties from six Chinese cities. The bars represent the**
200 **light absorption coefficient at 365 nm ($b_{\text{abs}365}$, left axis), and the lines represent the mass absorption efficiency**
201 **at 365 nm (MAE_{365} , right axis).**

202 The mass absorption efficiency (MAE , $\text{m}^2 \text{ g}^{-1}$) is a key parameter for describing the light absorption
203 ability of atmospheric BrC (Li et al., 2021; Peng et al., 2020). Figure 2 illustrated the average MAE
204 values measured at 365 nm (MAE_{365}) in the six cities; compared with the value measured in CD ($0.37 \pm$
205 $0.18 \text{ m}^2 \text{ g}^{-1}$), those measured in the other five cities were higher by 1.1–3.3 times. These cities can be
206 arranged as follows (in descending order) in terms of the measured MAE_{365} values: HrB > BJ > WH >
207 XA > GZ > CD. These differences in MAE_{365} values can be attributed to the variance of the light

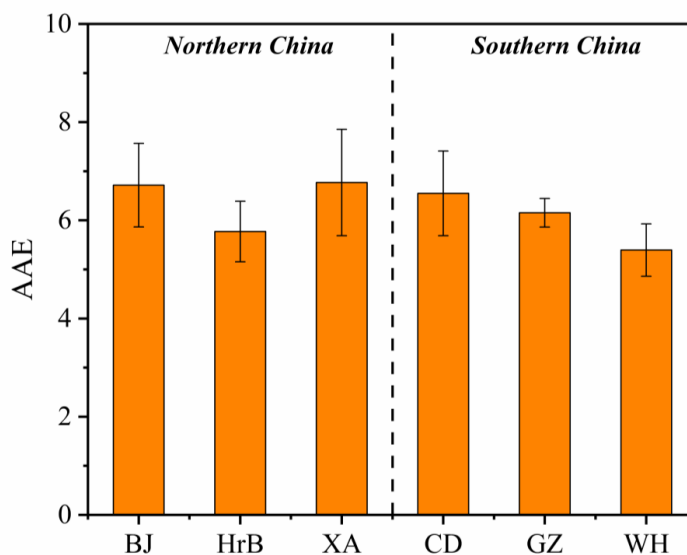


208 absorption capacity of BrC in different megacities. The average MAE₃₆₅ values measured for BrC in BJ,
209 HrB, XA, and WH (range: 0.68–1.21 m² g⁻¹) were within the MAE ranges of biomass burning, such as,
210 the average MAE₃₆₅ measured for BrC were 0.97 ± 0.26 m² g⁻¹ for wood burning (Du et al., 2014), 1.05
211 ± 0.08 m² g⁻¹ for corn stalk combustion (Du et al., 2014), and 1.28 ± 0.12 m² g⁻¹ for wheat stubble burning
212 (Xie et al., 2017; Lei et al., 2018), indicating that biomass burning may be a major source of winter BrC
213 in these cities. Biomass burning is commonly regarded as the main emission source for BrC, which has
214 a high absorption capacity, as indicated by field observations and model predictions (Desyaterik et al.,
215 2013; Feng et al., 2013; Lei et al., 2018). Notably, the MAE₃₆₅ values derived for BrC emitted from
216 primary fossil fuel combustion are similar to those derived for biomass burning (Yan et al., 2017); for
217 example, former studies have revealed that the MAE₃₆₅ values for BrC produced by primary emissions
218 from residential coal combustion were in the range of 0.30–1.51 m² g⁻¹ (Ni et al., 2021; Yan et al., 2017).
219 Therefore, coal combustion may also be a potential source of BrC in these cities. By contrast, we
220 observed lower average MAE₃₆₅ values for BrC in GZ and CD (range: 0.37–0.39 m² g⁻¹). Previous studies
221 have revealed relatively low MAE values for BrC from motor vehicle emissions, including gasoline
222 vehicle emissions (0.62 ± 0.76 m² g⁻¹; Xie et al., 2017) and motorcycle emissions (0.20 ± 0.08 m² g⁻¹;
223 Du et al., 2014). These findings suggest that the BrC sampled in GZ and CD mainly originated from
224 traffic emissions. In addition, laboratory experiments in a previous study revealed that MAE₃₆₅ values
225 decreased from 1.43 to 0.11 m² g⁻¹ with aerosol aging, which suggests the production of SOA (Ni et al.,
226 2021). This finding demonstrates that secondary formation processes are among the main sources of BrC
227 in CD and GZ.

228 The absorption Ångström exponent (AAE) measurements at 330–550 nm represents the wavelength
229 dependence of light absorption by BrC (Cheng et al., 2017). We observed that the average AAE values
230 for BrC varied from 5.4 to 6.8 in the six cities (Figure 3). In general, the AAE values obtained in this
231 study are higher than those obtained at the Nepal Climate Observatory-Pyramid (3.7–4.0; Kirillova et al.,
232 2016) and in the Los Angeles Basin (4.82 ± 0.49; Zhang et al., 2013) and lower than those obtained at
233 the Tibetan Plateau (8.2 ± 1.4; Zhu et al., 2018). Nevertheless, the values obtained in this study are
234 comparable to those obtained in Beijing (5.3–7.3; Cheng et al., 2016; Wu et al., 2021), Nanjing (6.7;
235 Chen et al., 2018), the Indo-Gangetic Plain (5.3; Srinivas et al., 2016), New Delhi (5.1; Kirillova et al.,
236 2014), Seoul (5.5–5.8; Kim et al., 2016), and Xi'an (5.3–6.1; Huang et al., 2018). These similarities can
237 primarily be attributed to the consistent solubility of chromophores, which are sensitive to the type of



238 fuel used, the combustion conditions, and the solvents used (Cao et al., 2021; Huo et al., 2018).
239 Furthermore, the AAE values obtained in this study are within the range of those reported by previous
240 studies for coal combustion (5.5–6.4; Ni et al., 2021), biomass burning (4.4–8.7; Xie et al., 2017), and
241 gasoline vehicle emissions (6.2–6.9; Xie et al., 2017). This suggests that BrC in our study may have
242 multiple sources. Additionally, in contrast to the trends observed for the $b_{\text{abs}365}$ and MAE_{365} values for
243 BrC in the various cities, the AAE values observed in CD and GZ were higher than those observed in the
244 other cities. A previous study reported that the AAE values for SOA were higher than those for primary
245 organic aerosols (Saleh et al., 2013), and previous laboratory combustion experiments revealed that the
246 aging of biomass burning aerosols generally engenders an increase in AAE values (from 6.93 to 15.59;
247 Sengupta et al., 2018). These findings suggest that BrC in the cities in this study was also affected by
248 secondary formation processes.



249

250 **Figure 3.** AAE values of BrC in six cities. AAE is calculated between 330 and 550 nm.

251 3.3 Molecular structure of BrC

252 In order to further explore the reasons for the differences in the optical properties of BrC among these
253 cities, the functional groups of BrC were measured using FT-IR spectroscopy. Figure 4 illustrates the FT-
254 IR spectra of BrC fractions within the region of 4000–400 cm^{-1} in the six cities. The band in the region
255 of 400–800 cm^{-1} resulted from the interference from water vapor inside the instrument and thus can be



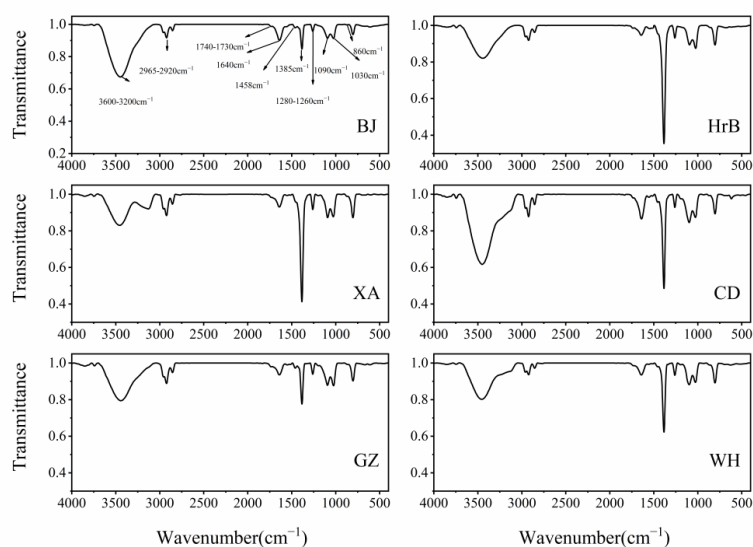
256 ignored (Zhang et al., 2020). The broad and strong peak at 3450 cm^{-1} was contributed to the O-H stretch
257 of H-bonded hydroxyl groups, phenols and carboxylic (Fan et al., 2016; Mukherjee et al., 2020). The
258 sharp band near 1740 cm^{-1} was usually assigned to the C=O bonds of ketones, quinones, and amides
259 (Duarte et al., 2005; Kristensen et al., 2015). We also attributed the sharp and intense absorption peaks
260 at $2850\text{--}2990\text{ cm}^{-1}$ to aliphatic asymmetric and symmetric C-H stretching vibrations (Coury and Dillner,
261 2008). Some bands were also displayed near 1385 , 1458 and 1640 cm^{-1} , indicating the presence of
262 aromatic groups (Fan et al., 2016; Zhao et al., 2022). These results demonstrate the complexity of the
263 chemical composition of BrC in the six cities, mainly containing aliphatic chains, carboxylic groups, and
264 aromatic groups.

265 In contrast to these similar functional groups, the apparent differences of typical functional bands were
266 also found among these cities. The strong band near 3130 cm^{-1} denoting O-H band (Fan et al., 2016;
267 Mukherjee et al., 2020) were only detected in XA, CD and WH, and the same peak were observed in the
268 spectra from the corn straw burning (Fan et al., 2016) and coal combustion (Zhang et al., 2022), which
269 stressed the emissions of biomass burning and coal combustion with high abundance of oxygenated
270 phenolic compounds in these cities. Moreover, it was noted that the peaks at 1640 , 1458 , 1385 and 1030
271 cm^{-1} was significantly higher in HrB, XA and WH than those in other cities. Previous studies confirmed
272 that these bands were generally ascribed to the C=C and C-H stretching of aromatic rings, O-H bond
273 deformation and C-O stretching of phenolic groups (Fan et al., 2016; Mukherjee et al., 2020). These
274 observations indicated the contribution of biomass burning to BrC in winter; this was because that
275 biomass burning can release heat-modified lignin derivatives such as aromatic phenols (e.g., syringyl
276 and guaiacyl) (Duarte et al., 2007; Fan et al., 2016; Zhao et al., 2022). Previous studies have shown that
277 BrC from biomass burning has a high light absorption capacity (Cao et al., 2021; Desyaterik et al., 2013;
278 Kumar et al., 2018), which supported that these cities with higher abundance of aromatic phenol
279 functional groups were consisted with higher $b_{\text{abs}365}$ (range: $8.3\text{--}29.3\text{ Mm}^{-1}$) and MAE₃₆₅ (range: 0.68--
280 $1.21\text{ m}^2\text{ g}^{-1}$) values in section 3.2.

281 Furthermore, we observed three peaks at 860 , $1280\text{--}1260$, and 1640 cm^{-1} , demonstrating the presence
282 of organic-nitrate (C-ONO₂) and oxygenated phenolic groups (Day et al., 2010; Zhang et al., 2020).
283 Previous studies have shown that the anthropogenic volatile organic compounds, sulfates, nitrates and
284 other acidic particle components from coal and biomass combustion may enhance the contents of these
285 functional groups through aqueous-phase formation under high humidity conditions (Gilardoni et al.,



286 2016; Wang et al., 2019; Zhang et al., 2020). Therefore, the FT-IR spectra indicated that all the BrC
287 samples from six cities have the contribution of secondary generation. Besides, the abundance of
288 functional groups at these wavenumbers, especially at 1640 cm^{-1} , was higher in CD than that in other
289 cities. These results might indicate that the secondary source of BrC was relatively high in CD.



290
291 **Figure 4. FTIR spectra of BrC in six megacities.**

292 **3.4 Source apportionment of BrC**

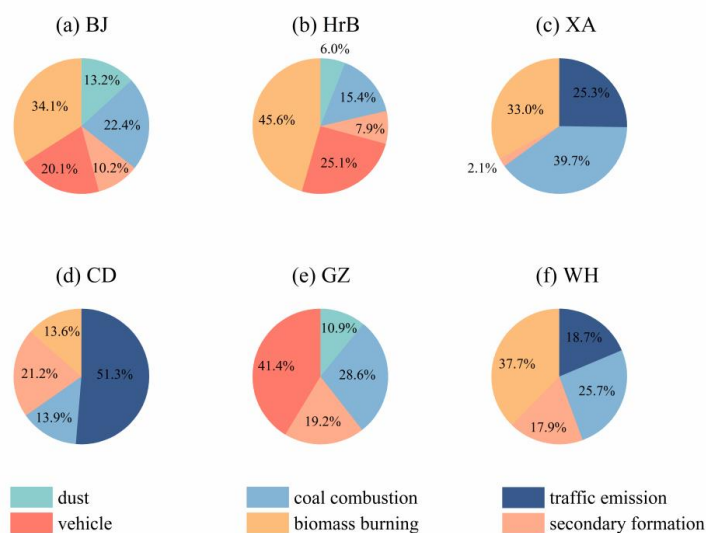
293 Considering the complexity of atmospheric processes, and the correlation and/or nonlinear interaction
294 between independent variables (i.e., multicomponent or multi-source interactions), we attempted to apply
295 ANN techniques of nonlinear functions, such as MLP model, combined PMF analysis to predict the
296 source contribution of allocated BrC from $\text{PM}_{2.5}$ sources in this study. The PMF-apportioned source
297 contributions to $\text{PM}_{2.5}$ in the six cities are presented in Figures S4 and S5. A strong linear correlation was
298 observed between the measured and PMF-reconstructed $\text{PM}_{2.5}$ mass concentrations ($r = 0.90\text{--}0.99$ in the
299 six cities), demonstrating the validity and robustness of our PMF solutions. As illustrated in Figure S4,
300 the first source was dominated by sulfate, OC, and EC and was considered to represent from coal
301 combustion (Huang et al., 2014). The second source comprised high concentrations of NH_4^+ , NO_3^- , and
302 SO_4^{2-} and was considered to represent secondary formation processes (Shen et al., 2010). Furthermore,
303 the third source comprised high loadings of K^+ and was considered to represent biomass burning (Shen



304 et al., 2010). The fourth source primarily comprised Na^+ , Mg^{2+} , and Ca^{2+} and was thus determined to
305 represent fugitive dust (Shakeri et al., 2016; Shen et al., 2016; Sun et al., 2019). The fifth source contained
306 high concentrations of Mg^{2+} , Ca^{2+} , NO_3^- , OC, and EC and was thus identified as representing traffic-
307 related emissions (Shakeri et al., 2016). Finally, the sixth source comprised high concentrations of OC,
308 EC, and NO_3^- and was considered to represent vehicle emissions (Shakeri et al., 2016).

309 The optimal neural network model for each site were explored by changing activation function types
310 (Tan H and Sigmoid), optimizing algorithms (scaled conjugate and gradient descent), and based on the
311 lowest root mean square error (RMSE) and the highest correlation coefficient (r) between observed and
312 MLP-modelled values (Borlaza et al., 2021). Although there are other architectures that are more
313 complex for MLP models, a basic MLP architecture was considered sufficient for the input and output
314 data sets of this study.

315 Figure S6 shows the correlation between observed values and BrC $b_{\text{abs}365}$ predicted values from
316 selected MLP models. The good correlation indicated the reliability of the model results. On the basis of
317 the MLP results, we calculated the source-specific contributions to BrC in the six cities (Figure 5). The
318 primary sources including coal combustion, dust, vehicle, biomass burning and traffic emissions, and
319 their average contribution to BrC in the northern cities was 93.3%, which was 1.2 times higher than that
320 in the southern cities. Among these primary emissions, we noted that a higher contribution of biomass
321 burning to BrC in HrB, BJ, XA and WH compared to other cities, which is consistent with the higher
322 abundance of biomass burning products, such as aromatic phenol functional groups was founded in these
323 cities as discussed in section 3.3. As supported, the BrC from biomass burning have high MAE₃₆₅ values
324 (Cao et al., 2021; Kumar et al., 2018), which can be also observed among these cities (range: 0.68–1.20
325 $\text{m}^2 \text{g}^{-1}$). On average, the secondary formation source contribution to BrC in southern cities was 19.4%,
326 which was 2.9 times higher than that in northern cities. Besides, the highest contribution was observed
327 in CD with 21.2%, followed by GZ > WH > BJ > HrB > XA. This result can be supported by the
328 abundance of organic-nitrate functional groups, the relatively high AAE value and low MAE₃₆₅ value in
329 CD, which were closely related with the contribution of secondary sources.



330
331 **Figure 5. The source contribution to BrC using multilayer perceptron neural network analysis in (a) BJ, (b)**
332 **HrB, (c) XA, (d) CD, (e) GZ, (f) WH.**

333 4 Conclusions

334 We investigated the sources and light absorption properties of BrC in wintertime in six megacities
335 across China. Both the b_{abs} and MAE_{365} of BrC at 365 nm in northern cities were approximately 2.5 and
336 1.8 times higher than those in southern cities. The MAE_{365} values measured for BrC in BJ, HrB, XA and
337 WH were ranged from 0.68 to 1.21 $\text{m}^2 \text{g}^{-1}$, which were within the MAE ranges derived for biomass
338 burning. Thus, these comparisons confirmed that emissions from biomass burning might be the major
339 BrC source in winter in these cities. Previous studies have reported that MAE_{365} values decreased with
340 aerosol aging while the AAE values of SOA were higher than those for POA. Besides, we noticed that
341 the average MAE_{365} and AAE values showed different trends in southern cities of CD and GZ, that is,
342 the MAE_{365} values of these two cities were lower than those of other cities, while the AAE values were
343 relatively higher. These evidences supported the secondary formation process were among the main
344 sources of BrC in CD and GZ.

345 The chemical functional groups of BrC in six cities mainly included aliphatic chains, carboxyl groups
346 and aromatic groups. However, the apparent difference of typical functional bands revealed the important



347 contributions of primary biomass burning and coal combustion to BrC for high abundance of oxygenated
348 phenolic compounds in these cities, especially in HrB, XA and WH. In contrast, the presence of organic-
349 nitrate (C-ONO₂) and oxygenated phenolic groups in BrC molecular implied the contribution from
350 secondary formation in six megacities, especially in CD city.

351 Due to the complexity of atmospheric processes, which are usually non-linear in nature, and the
352 traditional linear-based source analytic models may be limited. Here, we used a multilayer perceptron
353 (MLP) model based on artificial neural network (ANN) to improve the source allocation of BrC in these
354 cities. Source apportionment of BrC based on PMF and ANN-MLP analysis revealed that primary
355 emissions (e.g., biomass burning, coal combustion, and vehicle emissions) were key contributors to BrC,
356 and their average contribution in northern cities was about 93.3%, which was 1.2 times higher than that
357 in southern cities. Secondary formation processes made a greater contribution to BrC in southern cities
358 (19.4%) than northern cities (6.7%). The results of our work can provide a basis for the development of
359 more effective practices to control BrC emissions at the regional level.

360

361 **Data availability.** The key data sets are publicly available on the Zendo data repository platform:
362 <https://zenodo.org/record/6790321>.

363

364 **Author contribution.** ZS: Conceptualization. DW, TZ, and SH: Data curation. ZS and HX: Funding
365 acquisition. DW and YL: Methodology. ZS and JC: Resources. DW: Writing - original draft. DW, ZS,
366 QZ, HX, JS, JC and YL: Writing - review & editing.

367

368 **Competing interests.** The authors declare that they have no conflict of interest.

369

370 **Acknowledgements.** This research was supported by the National Natural Science Foundation of China
371 (41877383) and State Key Laboratory of Loess and Quaternary Geology, Institute of Earth Environment,
372 CAS (SKLLQG2103). Authors also thanks for Dr. Jun Tao, Renjian Zhang, Shaofei Kong, and Song Cui
373 for their help in field sampling.

374 **References**



375 Bao, M., Zhang, Y. L., Cao, F., Lin, Y. C., Hong, Y., Fan, M., Zhang, Y., Yang, X., and Xie, F.: Light
376 absorption and source apportionment of water soluble humic-like substances (HULIS) in PM_{2.5} at
377 Nanjing, China, *Environ. Res.*, 206, 112554, <https://doi.org/10.1016/j.envres.2021.112554>, 2022.

378 Borlaza, L. J. S., Weber, S., Jaffrezo, J.-L., Houdier, S., Slama, R., Rieux, C., Albinet, A., Micallef, S.,
379 Trébluchon, C., and Uzu, G.: Disparities in particulate matter (PM₁₀) origins and oxidative potential at a
380 city scale (Grenoble, France) – Part 2: Sources of PM₁₀ oxidative potential using multiple linear
381 regression analysis and the predictive applicability of multilayer perceptron neural network analysis,
382 *Atmos. Chem. Phys.*, 21, 9719-9739, <https://doi.org/10.5194/acp-21-9719-2021>, 2021.

383 Cao, J. J., Lee, S. C., Ho, K. F., Zou, S. C., Fung, K., Li, Y., Watson, J. G., and Chow, J. C.: Spatial and
384 seasonal variations of atmospheric organic carbon and elemental carbon in Pearl River Delta Region,
385 China, *Atmos. Environ.*, 38, 4447-4456, <https://doi.org/10.1016/j.atmosenv.2004.05.016>, 2004.

386 Cao, J. J., Wang, Q. Y., Chow, J. C., Watson, J. G., Tie, X. X., Shen, Z. X., Wang, P., and An, Z. S.:
387 Impacts of aerosol compositions on visibility impairment in Xi'an, China, *Atmos. Environ.*, 59, 559-566,
388 <https://doi.org/10.1016/j.atmosenv.2012.05.036>, 2012.

389 Cao, T., Li, M., Zou, C., Fan, X., Song, J., Jia, W., Yu, C., Yu, Z., and Peng, P. a.: Chemical composition,
390 optical properties, and oxidative potential of water- and methanol-soluble organic compounds emitted
391 from the combustion of biomass materials and coal, *Atmos. Chem. Phys.*, 21, 13187-13205,
392 <https://doi.org/10.5194/acp-21-13187-2021>, 2021.

393 Chen, D., Zhao, Y., Lyu, R., Wu, R., Dai, L., Zhao, Y., Chen, F., Zhang, J., Yu, H., and Guan, M.: Seasonal
394 and spatial variations of optical properties of light absorbing carbon and its influencing factors in a typical
395 polluted city in Yangtze River Delta, China, *Atmos. Environ.*, 199, 45-54,
396 <https://doi.org/10.1016/j.atmosenv.2018.11.022>, 2019.

397 Chen, Y., Ge, X., Chen, H., Xie, X., Chen, Y., Wang, J., Ye, Z., Bao, M., Zhang, Y., and Chen, M.:
398 Seasonal light absorption properties of water-soluble brown carbon in atmospheric fine particles in
399 Nanjing, China, *Atmos. Environ.*, 187, 230-240, <https://doi.org/10.1016/j.atmosenv.2018.06.002>, 2018.

400 Cheng, Y., He, K. B., Engling, G., Weber, R., Liu, J. M., Du, Z. Y., and Dong, S. P.: Brown and black
401 carbon in Beijing aerosol: Implications for the effects of brown coating on light absorption by black
402 carbon, *Sci. Total Environ.*, 599-600, 1047-1055, <https://doi.org/10.1016/j.scitotenv.2017.05.061>, 2017.

403 Cheng, Y., He, K. B., Du, Z. Y., Engling, G., Liu, J. M., Ma, Y. L., Zheng, M., and Weber, R. J.: The
404 characteristics of brown carbon aerosol during winter in Beijing, *Atmos. Environ.*, 127, 355-364,



- 405 <https://doi.org/10.1016/j.atmosenv.2015.12.035>, 2016.
- 406 Chung, C. E., Kim, S. W., Lee, M., Yoon, S. C., and Lee, S.: Carbonaceous aerosol AAE inferred from
407 in-situ aerosol measurements at the Gosan ABC super site, and the implications for brown carbon aerosol,
408 *Atmos. Chem. Phys.*, 12, 6173-6184, <https://doi.org/10.5194/acp-12-6173-2012>, 2012.
- 409 Coury, C. and Dillner, A. M.: A method to quantify organic functional groups and inorganic compounds
410 in ambient aerosols using attenuated total reflectance FTIR spectroscopy and multivariate chemometric
411 techniques, *Atmos. Environ.*, 42, 5923-5932, <https://doi.org/10.1016/j.atmosenv.2008.03.026>, 2008.
- 412 Day, D. A., Liu, S., Russell, L. M., and Ziemann, P. J.: Organonitrate group concentrations in submicron
413 particles with high nitrate and organic fractions in coastal southern California, *Atmos. Environ.*, 44, 1970-
414 1979, <https://doi.org/10.1016/j.atmosenv.2010.02.045>, 2010.
- 415 Desyaterik, Y., Sun, Y., Shen, X., Lee, T., Wang, X., Wang, T., and Collett, J. L.: Speciation of “brown”
416 carbon in cloud water impacted by agricultural biomass burning in eastern China, *J. Geophys. Res.*
417 *Atmos.*, 118, 7389-7399, <https://doi.org/10.1002/jgrd.50561>, 2013.
- 418 Devi, J. J., Bergin, M. H., McKenzie, M., Schauer, J. J., and Weber, R. J.: Contribution of particulate
419 brown carbon to light absorption in the rural and urban Southeast US, *Atmos. Environ.*, 136, 95-104,
420 <https://doi.org/10.1016/j.atmosenv.2016.04.011>, 2016.
- 421 Du, Z., He, K., Cheng, Y., Duan, F., Ma, Y., Liu, J., Zhang, X., Zheng, M., and Weber, R.: A yearlong
422 study of water-soluble organic carbon in Beijing II: Light absorption properties, *Atmos. Environ.*, 89,
423 235-241, <https://doi.org/10.1016/j.atmosenv.2014.02.022>, 2014.
- 424 Duarte, R. M. B. O., Pio, C. A., and Duarte, A. C.: Spectroscopic study of the water-soluble organic
425 matter isolated from atmospheric aerosols collected under different atmospheric conditions, *Anal. Chim.*
426 *Acta*, 530, 7-14, <https://doi.org/10.1016/j.aca.2004.08.049>, 2005.
- 427 Duarte, R. M. B. O., Santos, E. B. H., Pio, C. A., and Duarte, A. C.: Comparison of structural features of
428 water-soluble organic matter from atmospheric aerosols with those of aquatic humic substances, *Atmos.*
429 *Environ.*, 41, 8100-8113, <https://doi.org/10.1016/j.atmosenv.2007.06.034>, 2007.
- 430 Elangasinghe, M. A., Singhal, N., Dirks, K. N., and Salmond, J. A.: Development of an ANN-based air
431 pollution forecasting system with explicit knowledge through sensitivity analysis, *Atmos. Pollut. Res.*, 5,
432 696-708, <https://doi.org/10.5094/APR.2014.079>, 2014.
- 433 Elser, M., Huang, R.-J., Wolf, R., Slowik, J. G., Wang, Q., Canonaco, F., Li, G., Bozzetti, C., Daellenbach,
434 K. R., Huang, Y., Zhang, R., Li, Z., Cao, J., Baltensperger, U., El-Haddad, I., and Prévôt, A. S. H.: New



435 insights into PM_{2.5} chemical composition and sources in two major cities in China during extreme haze
436 events using aerosol mass spectrometry, *Atmos. Chem. Phys.*, 16, 3207-3225,
437 <https://doi.org/10.5194/acp-16-3207-2016>, 2016.

438 Fan, X., Wei, S., Zhu, M., Song, J., and Peng, P. a.: Comprehensive characterization of humic-like
439 substances in smoke PM_{2.5} emitted from the combustion of biomass materials and fossil fuels, *Atmos.*
440 *Chem. Phys.*, 16, 13321-13340, <https://doi.org/10.5194/acp-16-13321-2016>, 2016.

441 Feng, Y., Ramanathan, V., and Kotamarthi, V. R.: Brown carbon: a significant atmospheric absorber of
442 solar radiation?, *Atmos. Chem. Phys.*, 13, 8607-8621, <https://doi.org/10.5194/acp-13-8607-2013>, 2013.

443 Gilardoni, S., Massoli, P., Paglione, M., Giulianelli, L., Carbone, C., Rinaldi, M., Decesari, S., Sandrini,
444 S., Costabile, F., Gobbi, G. P., Pietrogrande, M. C., Visentin, M., Scotto, F., Fuzzi, S., and Facchini, M.
445 C.: Direct observation of aqueous secondary organic aerosol from biomass-burning emissions, *P. Natl.*
446 *Acad. Sci. USA.*, 113, <https://doi.org/10.1073/pnas.1602212113>, 2016.

447 Huang, R. J., Yang, L., Cao, J., Chen, Y., Chen, Q., Li, Y., Duan, J., Zhu, C., Dai, W., Wang, K., Lin, C.,
448 Ni, H., Corbin, J. C., Wu, Y., Zhang, R., Tie, X., Hoffmann, T., O'Dowd, C., and Dusek, U.: Brown
449 Carbon Aerosol in Urban Xi'an, Northwest China: The composition and light absorption properties,
450 *Environ. Sci. Technol.*, 52, 6825-6833, <https://doi.org/10.1021/acs.est.8b02386>, 2018.

451 Huang, X. H. H., Bian, Q. J., Louie, P. K. K., and Yu, J. Z.: Contributions of vehicular carbonaceous
452 aerosols to PM_{2.5} in a roadside environment in Hong Kong, *Atmos. Chem. Phys.*, 14, 9279-9293,
453 <https://doi.org/10.5194/acp-14-9279-2014>, 2014.

454 Huo, Y., Li, M., Jiang, M., and Qi, W.: Light absorption properties of HULIS in primary particulate matter
455 produced by crop straw combustion under different moisture contents and stacking modes, *Atmos.*
456 *Environ.*, 191, 490-499, <https://doi.org/10.1016/j.atmosenv.2018.08.038>, 2018.

457 Jo, D. S., Park, R. J., Lee, S., Kim, S.-W., and Zhang, X.: A global simulation of brown carbon:
458 implications for photochemistry and direct radiative effect, *Atmos. Chem. Phys.*, 16, 3413-3432,
459 <https://doi.org/10.5194/acp-16-3413-2016>, 2016.

460 Kim, H., Kim, J. Y., Jin, H. C., Lee, J. Y., and Lee, S. P.: Seasonal variations in the light-absorbing
461 properties of water-soluble and insoluble organic aerosols in Seoul, Korea, *Atmos. Environ.*, 129, 234-
462 242, <https://doi.org/10.1016/j.atmosenv.2016.01.042>, 2016.

463 Kirchstetter, T. W., Novakov, T., and Hobbs, P. V.: Evidence that the spectral dependence of light
464 absorption by aerosols is affected by organic carbon, *J. Geophys. Res. Atmos.*, 109,



- 465 <https://doi.org/10.1029/2004JD004999>, 2004.
- 466 Kirillova, E. N., Andersson, A., Tiwari, S., Srivastava, A. K., Bisht, D. S., and Gustafsson, Ö.: Water-
467 soluble organic carbon aerosols during a full New Delhi winter: Isotope-based source apportionment and
468 optical properties, *J. Geophys. Res. Atmos.*, 119, 3476-3485, <https://doi.org/10.1002/2013JD020041>,
469 2014.
- 470 Kirillova, E. N., Marinoni, A., Bonasoni, P., Vuillermoz, E., Facchini, M. C., Fuzzi, S., and Decesari, S.:
471 Light absorption properties of brown carbon in the high Himalayas, *J. Geophys. Res. Atmos.*, 121, 9621-
472 9639, <https://doi.org/10.1002/2016JD025030>, 2016.
- 473 Kristensen, T. B., Du, L., Nguyen, Q. T., Nøjgaard, J. K., Koch, C. B., Nielsen, O. F., Hallar, A. G.,
474 Lowenthal, D. H., Nekat, B., Pinxteren, D. v., Herrmann, H., Glasius, M., Kjaergaard, H. G., and Bilde,
475 M.: Chemical properties of HULIS from three different environments, *J. Atmos. Chem.*, 72, 65-80,
476 <https://doi.org/10.1007/s10874-015-9302-8>, 2015.
- 477 Kumar, N. K., Corbin, J. C., Bruns, E. A., Massabó, D., Slowik, J. G., Drinovec, L., Močnik, G., Prati,
478 P., Vlachou, A., Baltensperger, U., Gysel, M., El-Haddad, I., and Prévôt, A. S. H.: Production of
479 particulate brown carbon during atmospheric aging of residential wood-burning emissions, *Atmos. Chem.*
480 *Phys.*, 18, 17843-17861, <https://doi.org/10.5194/acp-18-17843-2018>, 2018.
- 481 Lambe, A. T., Cappa, C. D., Massoli, P., Onasch, T. B., Forestieri, S. D., Martin, A. T., Cummings, M. J.,
482 Croasdale, D. R., Brune, W. H., Worsnop, D. R., and Davidovits, P.: Relationship between oxidation level
483 and optical properties of secondary organic aerosol, *Environ. Sci. Technol.*, 47, 6349-6357,
484 <https://doi.org/10.1021/es401043j>, 2013.
- 485 Laskin, A., Laskin, J., and Nizkorodov, S. A.: Chemistry of atmospheric brown carbon, *Chem. Rev.*, 115,
486 4335-4382, <https://doi.org/10.1021/cr5006167>, 2015.
- 487 Lei, Y., Shen, Z., Wang, Q., Zhang, T., Cao, J., Sun, J., Zhang, Q., Wang, L., Xu, H., Tian, J., and Wu, J.:
488 Optical characteristics and source apportionment of brown carbon in winter PM_{2.5} over Yulin in Northern
489 China, *Atmos. Res.*, 213, 27-33, <https://doi.org/10.1016/j.atmosres.2018.05.018>, 2018.
- 490 Lei, Y., Shen, Z., Zhang, T., Lu, D., Zeng, Y., Zhang, Q., Xu, H., Bei, N., Wang, X., and Cao, J.: High
491 time resolution observation of PM_{2.5} Brown carbon over Xi'an in northwestern China: Seasonal variation
492 and source apportionment, *Chemosphere.*, 237, 124530,
493 <https://doi.org/10.1016/j.chemosphere.2019.124530.124530>, 2019.
- 494 Li, X., Zhao, Q., Yang, Y., Zhao, Z., Liu, Z., Wen, T., Hu, B., Wang, Y., Wang, L., and Wang, G.:



495 Composition and sources of brown carbon aerosols in megacity Beijing during the winter of 2016, *Atmos.*
496 *Res.*, 262, <https://doi.org/10.1016/j.atmosres.2021.105773>, 2021.

497 Ma, Y., Ye, J., Xin, J., Zhang, W., Vilà-Guerau de Arellano, J., Wang, S., Zhao, D., Dai, L., Ma, Y., Wu,
498 X., Xia, X., Tang, G., Wang, Y., Shen, P., Lei, Y., and Martin, S. T.: The stove, dome, and umbrella effects
499 of atmospheric aerosol on the development of the planetary boundary layer in hazy regions, *Geophys.*
500 *Res. Lett.*, 47, <https://doi.org/10.1029/2020GL087373>, 2020.

501 Mo, Y., Li, J., Cheng, Z., Zhong, G., Zhu, S., Tian, C., Chen, Y., and Zhang, G.: Dual carbon isotope-
502 based source apportionment and light absorption properties of water-soluble organic carbon in PM_{2.5} over
503 China, *J. Geophys. Res. Atmos.*, 126, <https://doi.org/10.1029/2020JD033920>, 2021.

504 Mukherjee, A., Dey, S., Rana, A., Jia, S., Banerjee, S., and Sarkar, S.: Sources and atmospheric
505 processing of brown carbon and HULIS in the Indo-Gangetic Plain: Insights from compositional analysis,
506 *Environ. Pollut.*, 267, 115440, <https://doi.org/10.1016/j.envpol.2020.115440>, 2020.

507 Ni, H., Huang, R. J., Pieber, S. M., Corbin, J. C., Stefenelli, G., Pospisilova, V., Klein, F., Gysel-Beer,
508 M., Yang, L., Baltensperger, U., Haddad, I. E., Slowik, J. G., Cao, J., Prevot, A. S. H., and Dusek, U.:
509 Brown carbon in primary and aged coal combustion emission, *Environ. Sci. Technol.*, 55, 5701-5710,
510 <https://doi.org/10.1021/acs.est.0c08084>, 2021.

511 Peng, C., Yang, F., Tian, M., Shi, G., Li, L., Huang, R. J., Yao, X., Luo, B., Zhai, C., and Chen, Y.: Brown
512 carbon aerosol in two megacities in the Sichuan Basin of southwestern China: Light absorption properties
513 and implications, *Sci. Total. Environ.*, 719, 137483, <https://doi.org/10.1016/j.scitotenv.2020.137483>,
514 2020.

515 Ram, K. and Sarin, M. M.: Day–night variability of EC, OC, WSOC and inorganic ions in urban
516 environment of Indo-Gangetic Plain: Implications to secondary aerosol formation, *Atmos. Environ.*, 45,
517 460-468, <https://doi.org/10.1016/j.atmosenv.2010.09.055>, 2011.

518 Saleh, R., Hennigan, C. J., McMeeking, G. R., Chuang, W. K., Robinson, E. S., Coe, H., Donahue, N.
519 M., and Robinson, A. L.: Absorptivity of brown carbon in fresh and photo-chemically aged biomass-
520 burning emissions, *Atmos. Chem. Phys.*, 13, 7683-7693, <https://doi.org/10.5194/acp-13-7683-2013>,
521 2013.

522 Satish, R., Rastogi, N., Singh, A., and Singh, D.: Change in characteristics of water-soluble and water-
523 insoluble brown carbon aerosols during a large-scale biomass burning, *Environ. Sci. Pollut. R.*, 27,
524 33339-33350, <https://doi.org/10.1007/s11356-020-09388-7>, 2020.



- 525 Sengupta, D., Samburova, V., Bhattarai, C., Kirillova, E., Mazzoleni, L., Iaukea-Lum, M., Watts, A.,
526 Moosmüller, H., and Khlystov, A.: Light absorption by polar and non-polar aerosol compounds from
527 laboratory biomass combustion, *Atmos. Chem. Phys.*, 18, 10849-10867, [https://doi.org/10.5194/acp-18-](https://doi.org/10.5194/acp-18-10849-2018)
528 10849-2018, 2018.
- 529 Shakeri, A., Madadi, M., and Mehrabi, B.: Health risk assessment and source apportionment of PAHs in
530 industrial and bitumen contaminated soils of Kermanshah province; NW Iran, *Toxicology and*
531 *Environmental Health Sciences*, 8, 201-212, <https://doi.org/10.1007/s13530-016-0277-x>, 2016.
- 532 Shen, Z., Arimoto, R., Cao, J., Zhang, R., Li, X., Du, N., Okuda, T., Nakao, S., and Tanaka, S.: Seasonal
533 variations and evidence for the effectiveness of pollution controls on water-soluble inorganic species in
534 total suspended particulates and fine particulate matter from Xi'an, China, *J. Air. Waste. Manag. Assoc.*,
535 58, 1560-1570, <https://doi.org/10.3155/1047-3289.58.12.1560>, 2008.
- 536 Shen, Z., Cao, J., Arimoto, R., Han, Y., Zhu, C., Tian, J., and Liu, S.: Chemical Characteristics of Fine
537 Particles (PM₁) from Xi'an, China, *Aerosol. Sci. Tech.*, 44, 461-472,
538 <https://doi.org/10.1080/02786821003738908>, 2010.
- 539 Shen, Z., Cao, J., Arimoto, R., Han, Z., Zhang, R., Han, Y., Liu, S., Okuda, T., Nakao, S., and Tanaka, S.:
540 Ionic composition of TSP and PM_{2.5} during dust storms and air pollution episodes at Xi'an, China, *Atmos.*
541 *Environ.*, 43, 2911-2918, <https://doi.org/10.1016/j.atmosenv.2009.03.005>, 2009.
- 542 Shen, Z., Sun, J., Cao, J., Zhang, L., Zhang, Q., Lei, Y., Gao, J., Huang, R. J., Liu, S., Huang, Y., Zhu,
543 C., Xu, H., Zheng, C., Liu, P., and Xue, Z.: Chemical profiles of urban fugitive dust PM_{2.5} samples in
544 Northern Chinese cities, *Sci. Total. Environ.*, 569-570, 619-626,
545 <http://dx.doi.org/10.1016/j.scitotenv.2016.06.156>, 2016.
- 546 Shen, Z., Zhang, Q., Cao, J., Zhang, L., Lei, Y., Huang, Y., Huang, R. J., Gao, J., Zhao, Z., Zhu, C., Yin,
547 X., Zheng, C., Xu, H., and Liu, S.: Optical properties and possible sources of brown carbon in PM_{2.5} over
548 Xi'an, China, *Atmos. Environ.*, 150, 322-330, <http://dx.doi.org/10.1016/j.atmosenv.2016.11.024>, 2017.
- 549 Soleimanian, E., Mousavi, A., Taghvaei, S., Shafer, M. M., and Sioutas, C.: Impact of secondary and
550 primary particulate matter (PM) sources on the enhanced light absorption by brown carbon (BrC)
551 particles in central Los Angeles, *Sci. Total. Environ.*, 705,
552 <https://doi.org/10.1016/j.scitotenv.2019.135902>, 2020.
- 553 Sreekanth, V., Niranjan, K., and Madhavan, B. L.: Radiative forcing of black carbon over eastern India,
554 *Geophys. Res. Lett.*, 34, <https://doi.org/10.1029/2007GL030377>, 2007.



555 Srinivas, B., Rastogi, N., Sarin, M. M., Singh, A., and Singh, D.: Mass absorption efficiency of light
556 absorbing organic aerosols from source region of paddy-residue burning emissions in the Indo-Gangetic
557 Plain, *Atmos. Environ.*, 125, 360-370, <http://dx.doi.org/10.1016/j.atmosenv.2015.07.017>, 2016.

558 Sun, J., Shen, Z., Cao, J., Zhang, L., Wu, T., Zhang, Q., Yin, X., Lei, Y., Huang, Y., Huang, R. J., Liu, S.,
559 Han, Y., Xu, H., Zheng, C., and Liu, P.: Particulate matters emitted from maize straw burning for winter
560 heating in rural areas in Guanzhong Plain, China: Current emission and future reduction, *Atmos. Res.*,
561 184, 66-76, <http://dx.doi.org/10.1016/j.atmosres.2016.10.006>, 2017.

562 Sun, J., Shen, Z., Zhang, L., Lei, Y., Gong, X., Zhang, Q., Zhang, T., Xu, H., Cui, S., Wang, Q., Cao, J.,
563 Tao, J., Zhang, N., and Zhang, R.: Chemical source profiles of urban fugitive dust PM_{2.5} samples from
564 21 cities across China, *Sci. Total. Environ.*, 649, 1045-1053,
565 <https://doi.org/10.1016/j.scitotenv.2018.08.374>, 2019.

566 Tao, J., Zhang, L., Cao, J., Zhong, L., Chen, D., Yang, Y., Chen, D., Chen, L., Zhang, Z., Wu, Y., Xia, Y.,
567 Ye, S., and Zhang, R.: Source apportionment of PM_{2.5} at urban and suburban areas of the Pearl River
568 Delta region, south China - With emphasis on ship emissions, *Sci. Total. Environ.*, 574, 1559-1570,
569 <http://dx.doi.org/10.1016/j.scitotenv.2016.08.175>, 2017.

570 Wang, Y., Hu, M., Wang, Y., Zheng, J., Shang, D., Yang, Y., Liu, Y., Li, X., Tang, R., Zhu, W., Du, Z.,
571 Wu, Y., Guo, S., Wu, Z., Lou, S., Hallquist, M., and Yu, J. Z.: The formation of nitro-aromatic compounds
572 under high NO_x and anthropogenic VOC conditions in urban Beijing, China, *Atmos. Chem. Phys.*, 19,
573 7649-7665, <https://doi.org/10.5194/acp-19-7649-2019>, 2019.

574 Wu, C., Wang, G., Li, J., Li, J., Cao, C., Ge, S., Xie, Y., Chen, J., Li, X., Xue, G., Wang, X., Zhao, Z.,
575 and Cao, F.: The characteristics of atmospheric brown carbon in Xi'an, inland China: sources, size
576 distributions and optical properties, *Atmos. Chem. Phys.*, 20, 2017-2030, [https://doi.org/10.5194/acp-20-](https://doi.org/10.5194/acp-20-2017-2020)
577 2017-2020, 2020.

578 Wu, Y., Li, J., Jiang, C., Xia, Y., Tao, J., Tian, P., Zhou, C., Wang, C., Xia, X., Huang, R. J., and Zhang,
579 R.: Spectral absorption properties of organic carbon aerosol during a polluted winter in Beijing, China,
580 *Sci. Total. Environ.*, 755, 142600, <https://doi.org/10.1016/j.scitotenv.2020.142600>, 2021.

581 Xie, M., Hays, M. D., and Holder, A. L.: Light-absorbing organic carbon from prescribed and laboratory
582 biomass burning and gasoline vehicle emissions, *Sci. Rep.*, 7, 7318, [https://doi.org/10.1038/s41598-017-](https://doi.org/10.1038/s41598-017-06981-8)
583 06981-8, 2017.

584 Xie, X., Chen, Y., Nie, D., Liu, Y., Liu, Y., Lei, R., Zhao, X., Li, H., and Ge, X.: Light-absorbing and



585 fluorescent properties of atmospheric brown carbon: A case study in Nanjing, China, *Chemosphere.*, 251,
586 126350, <https://doi.org/10.1016/j.chemosphere.2020.126350>, 2020.

587 Yan, C., Zheng, M., Bosch, C., Andersson, A., Desyaterik, Y., Sullivan, A. P., Collett, J. L., Zhao, B.,
588 Wang, S., He, K., and Gustafsson, O.: Important fossil source contribution to brown carbon in Beijing
589 during winter, *Sci. Rep.*, 7, 43182, <https://doi.org/10.1038/srep43182>, 2017.

590 Yan, J., Wang, X., Gong, P., Wang, C., and Cong, Z.: Review of brown carbon aerosols: Recent progress
591 and perspectives, *Sci. Total. Environ.*, 634, 1475-1485, <https://doi.org/10.1016/j.scitotenv.2018.04.083>,
592 2018.

593 Yuan, W., Huang, R.-J., Yang, L., Guo, J., Chen, Z., Duan, J., Wang, T., Ni, H., Han, Y., Li, Y., Chen, Q.,
594 Chen, Y., Hoffmann, T., and O'Dowd, C.: Characterization of the light-absorbing properties,
595 chromophore composition and sources of brown carbon aerosol in Xi'an, northwestern China, *Atmos.*
596 *Chem. Phys.*, 20, 5129-5144, <https://doi.org/10.5194/acp-20-5129-2020>, 2020.

597 Zhang, Q., Li, Z., Shen, Z., Zhang, T., Zhang, Y., Sun, J., Zeng, Y., Xu, H., Wang, Q., Hang Ho, S. S.,
598 and Cao, J.: Source profiles of molecular structure and light absorption of PM_{2.5} brown carbon from
599 residential coal combustion emission in Northwestern China, *Environ. Pollut.*, 299, 118866,
600 <https://doi.org/10.1016/j.envpol.2022.118866>, 2022.

601 Zhang, Q., Shen, Z., Zhang, L., Zeng, Y., Ning, Z., Zhang, T., Lei, Y., Wang, Q., Li, G., Sun, J.,
602 Westerdahl, D., Xu, H., and Cao, J.: Investigation of primary and secondary particulate brown carbon in
603 two Chinese cities of Xi'an and Hong Kong in wintertime, *Environ. Sci. Technol.*, 54, 3803-3813,
604 <https://dx.doi.org/10.1021/acs.est.9b05332>, 2020.

605 Zhang, T., Shen, Z., Zeng, Y., Cheng, C., Wang, D., Zhang, Q., Lei, Y., Zhang, Y., Sun, J., Xu, H., Ho, S.
606 S. H., and Cao, J.: Light absorption properties and molecular profiles of HULIS in PM_{2.5} emitted from
607 biomass burning in traditional "Heated Kang" in Northwest China, *Sci. Total. Environ.*, 776, 146014,
608 <https://doi.org/10.1016/j.scitotenv.2021.146014>, 2021.

609 Zhang, X., Lin, Y. H., Surratt, J. D., and Weber, R. J.: Sources, composition and absorption Angstrom
610 exponent of light-absorbing organic components in aerosol extracts from the Los Angeles Basin, *Environ.*
611 *Sci. Technol.*, 47, 3685-3693, <https://doi.org/10.1021/es305047b>, 2013.

612 Zhang, X., Lin, Y.-H., Surratt, J. D., Zotter, P., Prévôt, A. S. H., and Weber, R. J.: Light-absorbing soluble
613 organic aerosol in Los Angeles and Atlanta: A contrast in secondary organic aerosol, *Geophys. Res. Lett.*,
614 38, <https://doi.org/10.1029/2011GL049385>, 2011.



- 615 Zhao, R., Zhang, Q., Xu, X., Wang, W., Zhao, W., Zhang, W., and Zhang, Y.: Light absorption properties
616 and molecular compositions of water-soluble and methanol-soluble organic carbon emitted from wood
617 pyrolysis and combustion, *Sci. Total. Environ.*, 809, 151136,
618 <https://doi.org/10.1016/j.scitotenv.2021.151136>, 2022.
- 619 Zhu, C. S., Cao, J. J., Huang, R. J., Shen, Z. X., Wang, Q. Y., and Zhang, N. N.: Light absorption
620 properties of brown carbon over the southeastern Tibetan Plateau, *Sci. Total. Environ.*, 625, 246-251,
621 <https://doi.org/10.1016/j.scitotenv.2017.12.183>, 2018.